BBA - Molecular Basis of Disease 1870 (2024) 167348

Contents lists available at ScienceDirect

BBA - Molecular Basis of Disease

journal homepage: www.elsevier.com/locate/bbadis

Loss of Fic causes progressive neurodegeneration in a *Drosophila* model of hereditary spastic paraplegia

Amanda G. Lobato [a,b,c], Natalie Ortiz-Vega [a,b,d], Tijana Canic [b,d], Xianzun Tao [a,b], Nika Bucan [e], Kai Ruan [a,b], Adriana P. Rebelo [f], Rebecca Schule [g,h], Stephan Zuchner [f], Sheyum Syed [i], R. Grace Zhai [a,b,*]

[a] Department of Neurology, University of Chicago, Chicago, IL, USA
[b] Department of Molecular and Cellular Pharmacology, University of Miami Miller School of Medicine, Miami, FL, USA
[c] Graduate Program in Human Genetics and Genomics, University of Miami Miller School of Medicine, Miami, FL, USA
[d] Graduate Program in Molecular and Cellular Pharmacology, University of Miami Miller School of Medicine, FL, USA
[e] Undergraduate Program in Neuroscience, University of Miami, Coral Gables, FL, USA
[f] Dr. John T. Macdonald Foundation Department of Human Genetics and John P. Hussman Institute for Human Genomics, University of Miami Miller School of Medicine, Miami, FL, USA
[g] Hertie Institute for Clinical Brain Research (HIH), Center of Neurology, University of Tübingen, Tübingen, Germany
[h] German Center for Neurodegenerative Diseases (DZNE), University of Tübingen, Tübingen, Germany
[i] Department of Physics, University of Miami, Coral Gables, FL, USA

A B S T R A C T

Hereditary Spastic Paraplegia (HSP) is a group of rare inherited disorders characterized by progressive weakness and spasticity of the legs. Recent newly discovered biallelic variants in the gene *FICD* were found in patients with a highly similar phenotype to early onset HSP. *FICD* encodes filamentation induced by cAMP domain protein. FICD is involved in the AMPylation and deAMPylation protein modifications of the endoplasmic reticulum (ER) chaperone BIP, a major constituent of the ER that regulates the unfolded protein response. Although several biochemical properties of FICD have been characterized, the neurological function of FICD and the pathological mechanism underlying HSP are unknown. We established a *Drosophila* model to gain mechanistic understanding of the function of FICD in HSP pathogenesis, and specifically the role of BIP in neuromuscular physiology. Our studies on *Drosophila* Fic null mutants uncovered that loss of *Fic* resulted in locomotor impairment and reduced levels of BIP in the motor neuron circuitry, as well as increased reactive oxygen species (ROS) in the ventral nerve cord of *Fic* null mutants. Finally, feeding *Drosophila* Fic null mutants with chemical chaperones PBA or TUDCA, or treatment of patient fibroblasts with PBA, reduced the ROS accumulation. The neuronal phenotypes of *Fic* null mutants recapitulate several clinical features of HSP patients and further reveal cellular patho-mechanisms. By modeling FICD in *Drosophila*, we provide potential targets for intervention for HSP, and advance fundamental biology that is important for understanding related rare and common neuromuscular diseases.

1. Introduction

Hereditary Spastic Paraplegia (HSP) is a diverse collection of Mendelian genetic disorders linked together by the clinical observations of lower limb weakness and spasticity [1,2]. HSPs may be caused by genetic variants that are autosomal dominant, autosomal recessive, X-linked, and in the mitochondrial genome [3,4]. HSP is classified clinically as “uncomplicated or pure” (non-syndromic) or “complicated” (syndromic), which accounts for 90 % or 10 % of patients, respectively. To date, variants in 73 genes have been found to link with HSP [4–6]. Due to the wide clinical and genetic heterogeneity of HSP, next generation sequencing approaches have increasingly been incorporated for genetic diagnostics in routine clinical settings [7].

A recent report has identified patients with newly discovered biallelic variants in the *FICD* gene causing a clinical phenotype consisting of a distinct slowly progressive motor neuron disease, reminiscent of hereditary spastic paraplegia with cerebellar dysfunction and peripheral neuropathy [6]. FICD, filamentation induced by cAMP domain protein, is responsible for AMPylation and deAMPylation of its substrate, BIP [8–13]. Binding immunoglobulin protein (BIP) is an Hsp70 protein folding chaperone located at the endoplasmic reticulum (ER) [14,15]. BIP is a major constituent of the ER and regulates the unfolded protein response in the endoplasmic reticulum (UPRER) by gene expression, oligomerization, and AMPylation [8,9,16–19]. AMPylation is a

* Corresponding author at: University of Chicago, Biological Sciences, Department of Neurology, 5841 South Maryland Avenue, MC 2030, Chicago, IL 60637, USA.
E-mail address: rgzhai@uchicago.edu (R.G. Zhai).

https://doi.org/10.1016/j.bbadis.2024.167348
Received 7 February 2024; Received in revised form 3 July 2024; Accepted 3 July 2024
Available online 8 July 2024

reversible and regulatory post-translational modification [20,21] that regulates BIP in translocating proteins into the ER, folding and holding protein substrates in the ER, initiating the unfolded protein response, and assisting in ER-associated degradation (ERAD) [15,22]. The endoplasmic reticulum (ER) plays a major role in maintaining protein homeostasis and is responsible for folding and processing nearly all polypeptides destined for secretion [19,23]. It is important to note that UPRER is essential for cell homeostasis, thus, any mutations to BIP or FICD will dramatically affect cellular physiology and pathology.

Although several biochemical properties of FICD have been characterized, the neurological function of FICD and the pathological mechanism underlying HSP are unknown. Given the complexity of the nervous phenotypes of HSP, in vivo modeling is required to dissect the pathomechanisms. *Drosophila* has been used successfully to model HSP (Table 1). For example, HSP caused by loss of Atlastin [24–26], loss of Rtn1 (reticulon) [27], and loss of Spastin [28] was successfully modeled in *Drosophila* and the underlying mechanisms were found to be involved in many processes including axonal transport, myelination, endomembrane trafficking, and mitochondria functions. HSP caused by loss of FICD emerged as a good candidate for modeling as *Drosophila* orthologue Dm Fic shares identical fic core domain and the salt bridge structure with human FICD, and thus, the AMPylation/deAMPylation functions are highly conserved. In this study, we established a *Drosophila* model to gain mechanistic understanding of the function of FICD in HSP pathogenesis, and specifically the role of BIP in neuromuscular physiology.

Table 1
Drosophila models of HSP. Disease column is classified by its SPG number. Type column is inheritance pattern of autosomal dominant (AD) or autosomal recessive (AR). Gene column is the name of the gene that corresponds to the disease. Protein column is the encoded protein by the gene. Function column is the function of the protein. Drosophila homolog column is the homolog for the human gene that is conserved in Drosophila. Phenotypes column is the previously characterized phenotypes in Drosophila for these proteins.

Disease	Type	Gene	Protein	Function [62]	*Drosophila* homolog	Phenotypes
SPG3A	AD	*ATL1*	Atlastin-1	ER morphogenesis and BMP signaling	*atl*	Muscle *atl* loss causes accumulation of aggregates containing polyubiquitin, decreased volume of endolysosomal network, and decreased lysosome number [63]. TrpA1 activation significantly decreased pupal size, and viability [64]. Adult flies show progressive decline in climbing ability [65]. *Atl* is required for normal growth of muscles and synapses at the neuromuscular junction [66]. *Atl* null flies were paralyzed by mechanical shock, and showed age-dependent degeneration of dopaminergic neurons [26].
SPG4	AD	*SPAST*	Spastin	Microtubule severing, ER morphogenesis, endosomal trafficking, BMP signaling	*spas*	At neuromuscular junctions, spastin RNAi causes morphological undergrowth and reduced synaptic area [67]. Neuromuscular junction synaptic boutons in *spastin* mutants are more numerous and more clustered than in wild-type, and transmitter release is impaired. *Spastin* null adult flies have severe movement defects and have short lifespans [68].
SPG7	AR	*SPG7*	Paraplegin	Mitochondrial m-AAA ATPase	*CG2658*	Mutants exhibited shortened lifespan, progressive locomotor defects, sensitivity to chemical and environmental stress, and muscular and neuronal degeneration. Also, altered axonal transport of mitochondria, reduced activities of respiratory chain complexes I and II, and severely swollen and dysmorphic mitochondria in the synaptic terminals of photoreceptors [69].
SPG10	AD	*KIF5A*	Kinesin heavy chain 5A	ATP-dependent motor that move cargoes in the anterograde direction along axons	*Khc*	Posterior paralysis, with organelle-filled axon swellings jammed with cargoes [2,62]. Mutants show disturbed axonal transport, altered structure and function of synapses, behavioral deficits, and increased mortality [70]. Glial-specific downregulation by RNAi suppresses neuronal excitability and results in spastic flies, as well as peripheral nerves swollen with maldistributed mitochondria [71].
SPG12	AD	*RTN2*	Reticulon 2	ER morphogenesis	*Rtn1*	Loss of *Rtn1* depleted ER membrane markers at the presynaptic motor terminals, reductions in activity-evoked Ca^{2+} fluxes in the cytosol, ER lumen, and mitochondria, as well as reduced evoked and spontaneous neurotransmission [72].
SPG15	AR	*ZFYVE26*	Spastizin	Endosomal trafficking, autophagy	*sptz/CG5270*	Autophagosome accumulation, enlarged lysosomes, reduced free lysosomes, and locomotor deficit [73].
SPG17	AD	*BSCL2*	Seipin	Lipid droplet biogenesis at ER	*seipin*	Mutant flies have reduced lipid storage in the fat body and accumulate ectopic lipid droplets in the salivary gland [74].
SPG20	AR	*SPART*	Spartin	Endosomal trafficking, BMP signaling, mitochondrial regulation	*spartin*	Loss of spartin induces age-dependent progressive defects of motor dysfunction and brain neurodegeneration [75].
SPG31	AD	*REEP1*	REEP1	ER morphogenesis and ER-microtubule interaction	*reepA*	ReepA is upregulated under stress conditions and aging. Lack of ReepA showed Atf6 and Ire1 activation, expansion of ER sheet-like structures, locomotor dysfunction, and shortened lifespan [76].
SPG35	AR	*FA2H*	Fatty acid 2-hydroxylase	Myelin lipid hydroxylation	*fa2h*	Loss of *fa2h* revealed behavioral abnormalities, in addition to a shortened lifespan. Alterations in mitochondrial dynamic and autophagy were identified [77].
SPG61	AR	*ARL6IP1*	ADP ribosylation factor-like GTPase 6-interacting protein 1	Connecting the ER and mitochondria as a member of MAMs	*Arl6IP1*	Loss of *Arl6IP1* results in progressive locomotor deficits and cell non-autonomous accumulation of lipid droplets in axonal glia [78]. Knockdown of *Arl6IP1* lowers Drp1 protein levels, resulting in reduced ER-mitochondrial contacts and impaired mitochondrial load at the distal ends of long motor neurons. *Arl6IP1* knockdown also demonstrate impaired autophagic flux and an accumulation of ubiquitinated proteins [79].

2. Results

2.1. Loss of Fic causes impaired locomotion

Recently discovered patients with Hereditary Spastic Paraplegia have biallelic variants in *FICD* [6], therefore we set out to characterize nervous system phenotypes associated with loss of Fic in *Fic* loss-of-function null mutant allele Fic^{30C} generated by a 101 bp deletion resulting in an early stop codon [12]. Fic^{30C} null mutants are viable and fertile with visual system defects [12,29]. Patients with biallelic variants in *FICD* have Hereditary Spastic Paraplegia, with common phenotypes of frequent falls, tiptoeing, walking difficulties, progressive unsteady gait, lower limb weakness, and motor neuropathy [6]. Modeling clinically relevant phenotypes is a gap of knowledge. *Drosophila* negative geotaxis behavior is ideal to model human movement and coordination [30,31]. To assess human disease relevant phenotypes, we recently established an innovative automated geotaxis monitoring system with computer-programmed motorized tapping and video tracking capabilities [32]. By extracting information about movement direction, speed, and climbing performance with sub-second resolution, we could dissect the most affected components of locomotor neurocircuitry in this model. Specifically, we quantitatively analyzed three features of the movement: speed, distance traveled, and movement direction. Individual fly vertical positions (maximum height, 14 cm) were used to calculate a cohort's climbing speed and total distance traveled. The difference in SD of horizontal (0°) and vertical (−90° and 90°) positions was used to calculate movement direction. Specifically, for a given fly, movement direction = (SD of y coordinates − SD of x coordinates)/(SD of y coordinates + SD of x coordinates).

To assess the age-dependent locomotor phenotype of Fic mutants, we first examined the locomotor activity in high resolution of female and male control flies (w^{1118}) and *Fic* null mutant flies (Fic^{30C}), at 5, 20, and 27 DAE (days after eclosion). Interestingly, *Fic* null mutant females have reduced movement direction (Fig. 1A), and reduced average speed (Fig. 1B) at all ages compared to their age-matched controls; while *Fic* null mutant males showed significant reduction of movement direction at 20 DAE (Fig. 1C), and reduced speed at 27 DAE compared to controls (Fig. 1D). When the distance traveled was analyzed using a kymograph, we found that the *Fic* null mutants, both males and females climb a shorter distance when compared to w^{1118} at all ages (Fig. 1E–J). Collectively, these results indicate that loss of *Fic* causes progressive locomotion impairment. Our results uncovered more severe and earlier onset movement phenotypes in females, suggesting a possible female vulnerability of loss of Fic.

2.2. Loss of Fic mutants recapitulate patient neurodegeneration phenotype

Patients with biallelic variants in *FICD* have common phenotypes of frequent falls, tiptoeing, walking difficulties, and progressive unsteady gait, all movement phenotypes associated with loss of coordination [6]. Normal *Drosophila* negative geotaxis behavior is a smooth upward motion that requires precise coordination, a lack of which results in falls and often followed by compensatory jumps [33–35]. To model disease-relevant coordination phenotype, we created a novel negative geotaxis monitoring output to track slips, falls, and jumps. Specifically, "slips" are defined as a negative (downward) distance between −4.7 to −11.7 mm, corresponding to 2–5 body-lengths of a fruit fly; "falls" are defined as a negative distance greater than −11.7 mm, corresponding to >5 body-lengths of a fruit fly; and "jumps" are defined as a positive (upward) distance >4.7 mm, corresponding to >2 body lengths of a fruit fly. The number of incidences of each event per climbing trial track was recorded and analyzed. For "slip" events, Fic^{30C} mutant females showed a significant, and progressive increase in slip incidence at 20 and 27 DAE, while Fic^{30C} mutant males showed an even earlier onset at 5 DAE (Fig. 2A–B). A representative distribution of the number of slip incidences at 20 DAE is shown in Fig. 2C, and other age-dependent time-points of 5 DAE and 27 DAE are respectively shown in Fig. S1A, S1B. For "fall" events, Fic^{30C} mutants showed a significant increase in incidence at 27 DAE for females, and an even earlier progressive phenotype starting at 20 DAE for males (Fig. 2D–E). A representative distribution of the number of fall incidences at 20 DAE is shown in Fig. 2F, and other age-dependent time-points of 5 and 27 DAE are respectively shown in Fig. S1C, D. Lastly, for "jump" events, Fic^{30C} mutants showed a significant increase starting at the earliest age of 5 DAE (Fig. 2G–H). A representative distribution of the number of jump incidences at 20 DAE is shown in Fig. 2I, and other age-dependent time-points of 5 DAE and 27

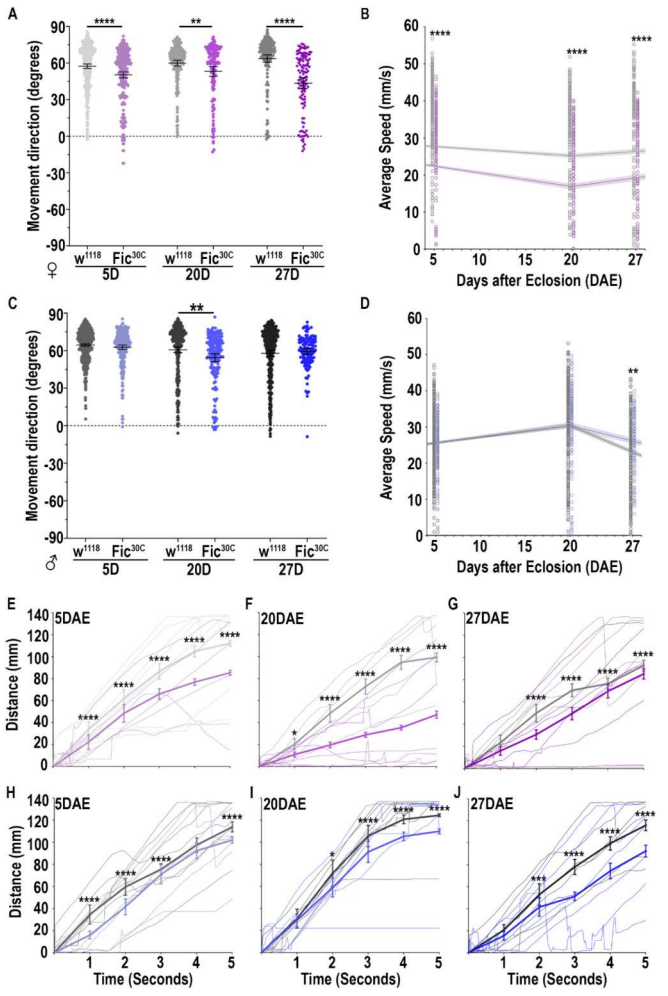

Fig. 1. Fic null flies have impaired locomotion. Locomotor activity of w^{1118} and Fic^{30C} females at 5DAE, 20DAE, and 27DAE for **(A)** movement direction (in degrees) and **(B)** average speed (in mm/s). Gray line is w^{1118} age-dependent mean speed with shaded area as confidence interval. Purple line is Fic^{30C} age-dependent mean speed with shaded area as confidence interval. Data are presented as mean ± 95 % CI, N = 120–420 tracks. Locomotor activity of w^{1118} and Fic^{30C} males at 5DAE, 20DAE, and 27DAE for **(C)** movement direction (in degrees) and **(D)** average speed (in mm/s). Gray line is w^{1118} age-dependent mean speed with shaded area as confidence interval. Blue line is Fic^{30C} age-dependent mean speed with shaded area as confidence interval. Data are presented as mean ± 95 % CI, N = 120–700 tracks. **(E–G)** Kymograph of climbing distance (in mm) for the first 5 s of w^{1118} (gray) and Fic^{30C} females (purple) at 5DAE, 20DAE, and 27DAE, respectively. Lighter background traces correspond to each fly in a vial for one trial with 10 tracks. Darker trace is the mean ± SD of all traces at each second. **(H–J)** Kymograph of climbing distance (in mm) for the first 5 s of w^{1118} (gray) and Fic^{30C} males (blue) at 5DAE, 20DAE, and 27DAE, respectively. Lighter background traces correspond to each fly in a vial for one trial with 10 tracks. Darker trace is the mean ± SD of all traces at each second. Student's t-test was performed for statistical analysis. $^{*}p < 0.05$, $^{**}p < 0.01$, $^{***}p < 0.001$, $^{****}p < 0.0001$.

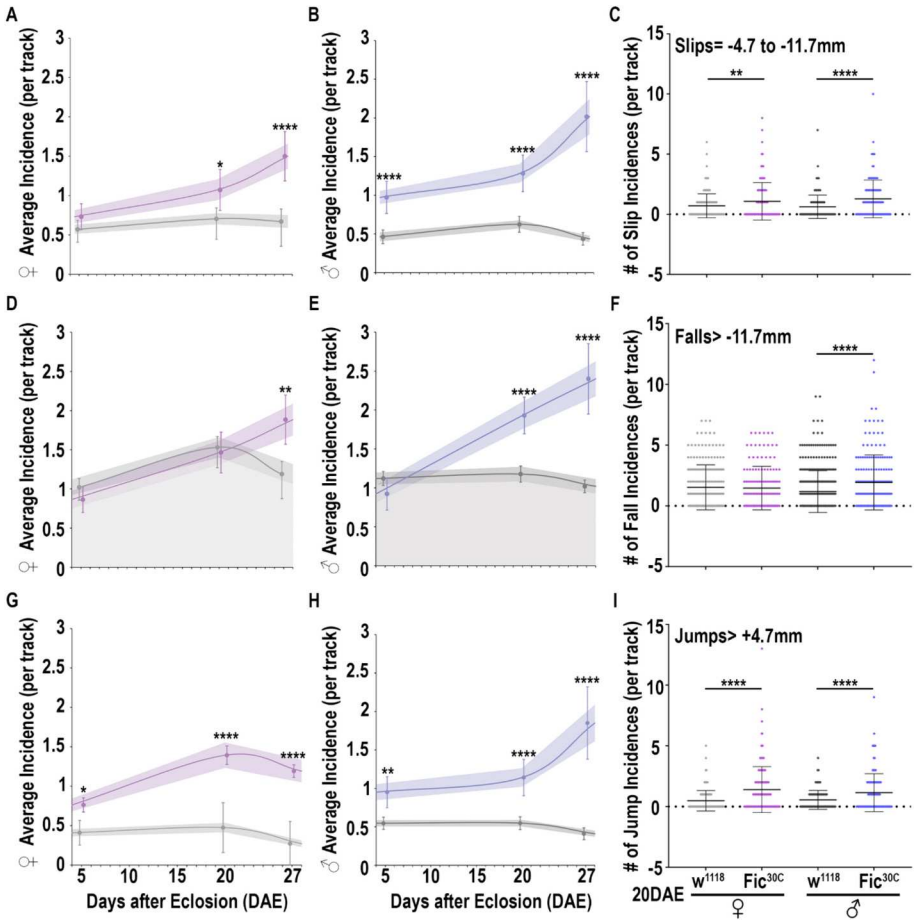

Fig. 2. Fic null flies recapitulate patient neurodegenerative phenotype. **(A)** Average incidence of slips (per track) for w^{1118} (gray) and Fic^{30C} (purple) females at 5DAE, 20DAE, and 27DAE. **(B)** Average incidence of slips (per track) for w^{1118} (gray) and Fic^{30C} (blue) males at 5DAE, 20DAE, and 27DAE. Data are presented as mean ± 95 % CI (shaded area), $N = 120–350$ tracks. **(C)** Representative distribution of the number of slip incidences (per track) at 20DAE. Data are presented as mean ± SD, $N = 140–340$ tracks. **(D)** Average incidence of falls (per track) for w^{1118} (gray) and Fic^{30C} (purple) females at 5DAE, 20DAE, and 27DAE. **(E)** Average incidence of falls (per track) for w^{1118} (gray) and Fic^{30C} (blue) males at 5DAE, 20DAE, and 27DAE. Data are presented as mean ± 95 % CI, N = 120–350 tracks. **(F)** Representative distribution of the number of fall incidences (per track) at 20DAE. Data are presented as mean ± SD, N = 140–340 tracks. **(G)** Average incidence of jumps (per track) for w^{1118} (gray) and Fic^{30C} (purple) females at 5DAE, 20DAE, and 27DAE. **(H)** Average incidence of jumps (per track) for w^{1118} (gray) and Fic^{30C} (blue) males at 5DAE, 20DAE, and 27DAE. Data are presented as mean ± 95 % CI, N = 120–350 tracks. **(I)** Representative distribution of the number of jump incidences (per track) at 20DAE. Data are presented as mean ± SD, N = 140–340 tracks. Student's *t*-test was performed for statistical analysis. *p < 0.05, **p < 0.01, ****$p < 0.0001$.

DAE are respectively shown in Fig. S1E, F. Taken together, the analysis of behavior coordination shows that loss of *Fic* resulted in a progressive deficiency of coordination and balance, reflected by increased frequency of slips and falls, and recovery jump attempts. These phenotypes closely track clinical presentations, and successfully recapitulate salient features of adult-onset, progressive movement phenotypes of Hereditary Spastic Paraplegia.

2.3. Loss of Fic leads to altered BIP levels and distribution in ventral nerve cord

Previous studies have demonstrated that FICD localizes to the ER and its primary target is the ER molecular chaperone binding immunoglobulin protein (BIP) [9,11,13]. BIP is expressed in all cells, including motor neurons, interneurons, and giant fiber neurons. To assess whether the unfolded protein response is being activated by BIP in an age-dependent manner, an immunofluorescence approach was used to observe endogenous BIP expression in the axon tracks including those of the giant fiber of the ventral nerve cord (Fig. 3A). To confirm the expression of BIP in large axon tracks including those of the giant fibers and to assess the giant fiber axon morphology in the ventral nerve cord, we expressed tdTomato and mitoGFP in the giant fiber using *R68A06-GAL4* [36], specifically expressed in the giant fiber neurons [37–39]. As shown in Fig. 3A, BIP positive puncta were detected in the axon and terminals in the medial VNC including the giant fiber axons, overlapping with the R68A06 positive tdTomato and mitoGFP signal.

We developed a novel method for analyzing BIP in the ventral nerve cord (Fig. S2A–D). The cell bodies of the giant fiber axons are located in the brain. ER has been shown to be present in the neuronal axons and synaptic terminals [40–42]. Given the large size and volume of cytoplasm in the long axons of large neurons such as human motor neurons and *Drosophila* giant fibers, analyzing the ER in the axons would be highly relevant to understanding axonal pathology in human motor neuron diseases. The anatomy of the *Drosophila* giant fiber axons is morphologically large and particularly feasible for this analysis. Furthermore, the *Drosophila* giant fiber neuron is homologous to human upper motor neurons [43,44]. Given the manifestation of FICD associated HSP in upper motor neurons [6], we focused on this area and carried out quantitative analysis on BIP localization.

After observing the pattern of giant fiber axons, we used their anatomical location to assess BIP patterns in our HSP model. When BIP expression in axon tracks in the ventral nerve cord including giant fiber

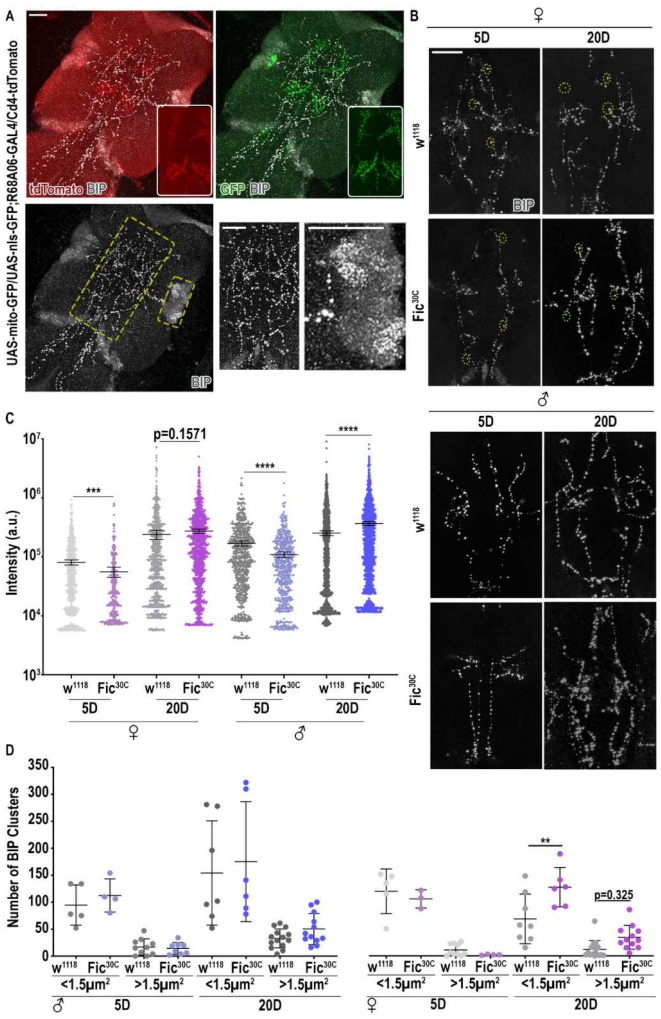

Fig. 3. Fic null flies have reduction of BIP at 5 DAE, followed by age-dependent increase of BIP at 20 DAE. **(A)** Ventral nerve cord of 5 DAE fly of genotype *UAS-mito-GFP/UAS-nls-GFP;R68A06-GAL4/Cd4-tdTomato* were dissected and stained for BIP (gray), as well as imaged for tdTomato (red) and GFP (green). Single channel of tdTomato and GFP are shown in their respective corners (boxed white areas) to highlight the giant fiber axons, as both tdTomato and mitoGFP were expressed in giant fiber neurons, driven by R68A06. Yellow boxed areas are zoom-in of the giant fiber axonal regions and the motor neuron cell body, respectively. **(B)** Ventral nerve cords of w^{1118} and Fic^{30C} females and males at 5 DAE and 20 DAE were dissected and stained for BIP (gray). **(C)** Quantification of BIP intensity. Data are presented as mean ± 95 % CI, $n = 3$–5, z-stacks of 15 sections were analyzed. Yellow dotted circles are examples of BIP clusters that were used for quantification. **(D)** Quantification of the distribution of BIP clusters for females and males at 5 DAE and 20 DAE. Data are presented as mean ± SD. Student's t-test was performed for statistical analysis. $^{**}p < 0.01$, $^{***}p < 0.001$, $^{****}p < 0.0001$. Scale bars (A-B): 30 μm.

axons was examined in control w^{1118} and Fic^{30C} flies at 5 and 20 DAE (Fig. 3B), we observed a significant decrease of BIP intensity at 5 DAE but an increase of BIP at 20 DAE in both female and male *Fic* null mutants compared to their respective controls (Fig. 3C), suggesting an age-dependent alteration of BIP in loss of Fic neurons. Next, we analyzed the clustering of BIP as a proxy for ER morphology. The endoplasmic reticulum has a mean size of 1 μm [45], hence, we separated BIP clusters into sizes of small ($<1.5\mu m^2$), and large ($>3\mu m^2$). We observed that at 20 DAE for *Fic* null females, there is a significant increase in small BIP clusters, and an increasing trend for large BIP clusters (Fig. 3D). Collectively, size distribution analysis of BIP clusters showed that BIP clustering is highly dynamic, consistent with an active role in the cellular unfolded protein response in the ER. The remarkable changes specifically in the population of small BIP clusters further indicate a critical role of Fic in regulating the dynamic cellular process of small BIP cluster formation.

2.4. Chemical chaperones reduce ROS accumulation in Fic null mutant tissue and HSP patient fibroblasts

The loss of proteostasis and subsequent accumulation of unfolded and misfolded proteins is a central molecular hallmark of aging and many degenerative diseases [23]. ER stress and activation of the unfolded protein response has been implicated in abnormal protein processing for the pathogenesis of these diseases, leading to the accumulation of reactive oxygen species (ROS) [46]. ROS are small, short-lived, and highly reactive molecules generated by the UPR-regulated oxidative folding machinery in the ER and in the mitochondria [47]. They can be free radicals derived from oxygen, including anionic superoxide or the hydroxyl radical, or nonradical molecule such as hydrogen peroxide [48]. The ER maintains a relatively high turn-over of reactive oxygen species as its oxidative protein folding machinery through disulfide bonds [49,50]. BIP has been identified as a redox signaling protein, and redox fluctuations within the ER can be detrimental to protein stability and homeostasis [48,51]. To analyze ROS levels in vivo, we performed live tissue staining with dihydroethidium (DHE). DHE staining can react with superoxide anions and form a red fluorescence, and has been widely used to evaluate ROS production in tissue and in vivo [52,53]. Quantitative imaging analysis of DHE fluorescence in female fly brain and ventral nerve cord showed a significant increase in *Fic* null flies, compared to that in control flies (Fig. 4A, B), suggesting an accumulation of ROS in the central nervous system of loss of Fic mutants.

Loss of Fic induced ER stress and accompanied ROS accumulation point to the unfolded protein and proteotoxic stress as a potential cellular target for FICD disease pathology. There have been several therapeutic compounds that have ameliorated phenotypes of *Drosophila* models of HSP (Table 2). To expand on this and to facilitate therapeutic discovery, we explored the beneficial effect of chemical chaperones. Chemical chaperones have been identified and implicated as potential treatments for ER-stress pathologies [54]. Chemical chaperones are low molecular weight compounds that mimic the functions of intracellular molecular chaperones by increasing the stability of native proteins and assisting refolding of unfolded polypeptides [55,56]. Two chemical chaperones approved by the US Food and Drug Administration, namely, 4-phenylbutyric acid (4-PBA) and tauroursodeoxycholic acid (TUDCA) are for clinical use in urea-cycle disorders in humans and as a liver-protecting agent in human cholestatic liver diseases, respectively [47,56]. Administration of PBA or TUDCA has been observed to reduce reactive oxygen species and endoplasmic reticulum stress, respectively, in *Drosophila* models [57,58].

To determine the effect of PBA or TUDCA on loss of Fic phenotypes in our HSP model, Fic^{30C} female mutant flies were fed with 2 mM PBA, 10 mM TUDCA, or vehicle (H_2O) containing food for 5 days, and compared to w^{1118} control flies (Fig. 4A, B). The dosing concentration of PBA, 2 mM, and TUDCA, 10 mM were selected and determined based on previous studies [57,58]. ROS accumulation and high-resolution negative geotaxis behavior were assessed as functional readouts. ROS accumulation in the brain of Fic^{30C} mutants was reduced with feeding of either chemical chaperone (Fig. 4C), while ROS accumulation in the ventral nerve cord of Fic^{30C} mutants was reduced only by PBA (Fig. 4D). The analysis of average speed showed an improvement at 5 DAE specifically with the chemical chaperone PBA (Fig. 4E), however, at a later stage, 27 DAE, drug treatment significantly reduced climbing speed in both control and Fic mutant flies, indicating a possible general toxicity of long-term treatment (Fig. 4E–F).

To explore the therapeutic potential of chemical chaperones for HSP and to expand our findings of ROS reduction in human cells, we evaluated the effect of PBA treatment on ROS level in FICD patient

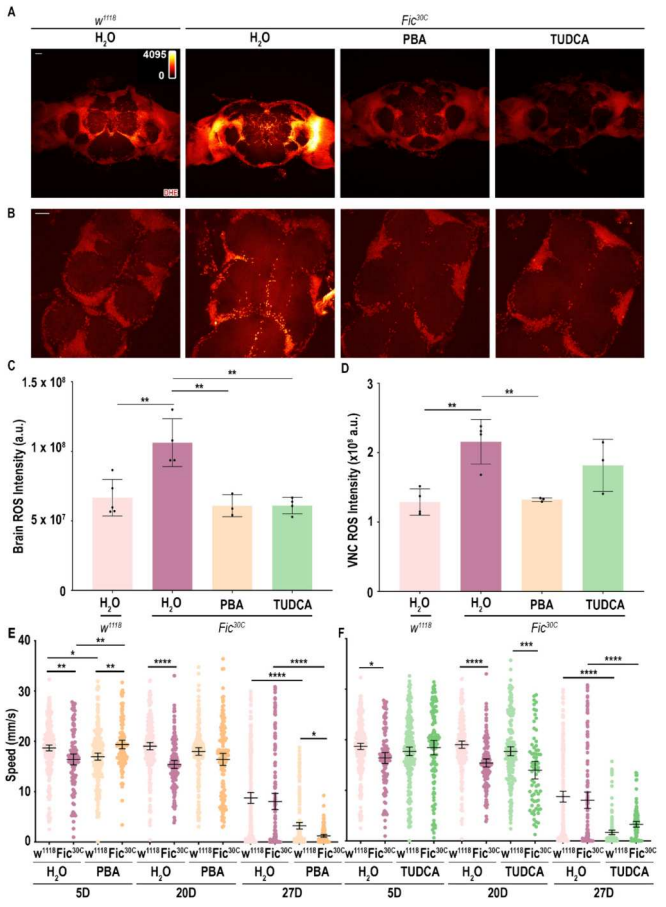

Fig. 4. Chemical chaperones reduce ROS accumulation in Fic null flies. **(A–B)** Live DHE staining of the brain **(A)** and ventral nerve cord **(B)** from female w^{1118} flies fed with H_2O, and Fic^{30C} flies fed with H_2O, PBA, or TUDCA at 5 DAE. Scale bars: 30 μm. Heatmap 0–4095. **(C–D)** Quantification of DHE fluorescent intensity in the brain **(C)** and VNC **(D),** respectively. Data are presented as mean ± SD, n = 3–5. **(E–F)** Average speed of w^{1118} and Fic^{30C} females fed with H_2O, PBA, or TUDCA at 5 DAE, 20 DAE, and 27 DAE. Data are presented as mean ± 95 % CI, N = 120–300 tracks. One-way ANOVA was performed for statistical analysis. *p < 0.05, **p < 0.01, ***p < 0.001, ****p < 0.0001.

fibroblasts. We assessed the cellular ROS with live imaging (Fig. 5A). Consistent with the findings from *Drosophila* nervous system, we observed a significant reduction of ROS intensity in patient-derived fibroblasts with PBA treatment (Fig. 5B). Collectively, these results indicate the initial beneficial effect of chemical chaperones, specifically PBA, for reducing reactive oxygen species accumulation and improving cellular health.

3. Discussion

Hereditary Spastic Paraplegias are a group of rare inherited disorders characterized by progressive weakness and spasticity of the legs. In this study, we established a *Drosophila* model to gain mechanistic understanding of the function of FICD in Hereditary Spastic Paraplegia pathogenesis. We discovered that *Fic* null flies have locomotor impairment recapitulating salient features of FICD patient neurodegenerative phenotypes. Our cellular analysis uncovered an age-dependent increase of BIP, accounting for the prolonged ER stress. Strikingly, alleviation of ER stress by reduction of reactive oxygen species with chemical chaperone PBA feeding, reversed this impact. By modeling FICD neurodegeneration in *Drosophila*, we provide mechanistic insights into disease pathology, uncover potential targets for intervention, and advance fundamental

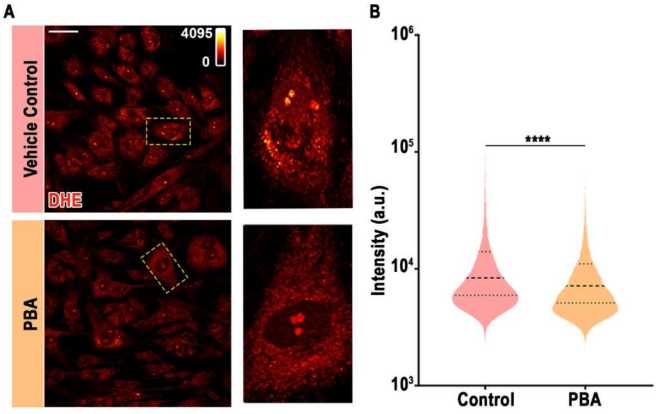

Fig. 5. PBA reduces ROS accumulation in patient-derived fibroblasts. **(A)** Live DHE staining in patient-derived fibroblasts. A series of six random microscopic fields were analyzed, and representative images are exhibited. Yellow-boxed rectangles show zoomed-in cell. Scale bar: 50 μm. Heatmap 0-4095. **(B)** Quantification of DHE fluorescent intensity in (**A**). Student's t-test was performed for statistical analysis. ****p < 0.0001.

Table 2
Therapeutic compounds for HSP. Treatment column describes which compound was tested. *Drosophila* HSP homolog column describes which model was used for testing the specific compound. The phenotype column describes which phenotypes were restored with treatment.

Treatment	*Drosophila* HSP homolog	Phenotype
Rapamycin	atl	Partially suppressed the behavioral consequences of both neuronal and muscle atl knockdown, and delayed polyubiquitin aggregate accumulation and degeneration of thoracic muscles [25,80].
Vinblastine		Alleviates synapse and muscle defects in atl mutants [66].
	spas	Increase in eclosion rate, improvement in locomotor ability and adult lifespan, increase in total synaptic area and decrease in bouton number [81].
Phenazine		Rescued the negative geotaxis defects caused by spastin loss of function [82].
Methylene blue		Rescued the negative geotaxis defects caused by spastin loss of function and re-adjusted the ER stress response biomarker levels back to wild-type [80,82].
N-acetyl-cysteine		Rescued the ER stress, lifespan, and locomotor defects [80,82].
Naringenin	reepA	Restores ER homeostasis, climbing capacity, and lifespan defects [76].
Liver X receptor agonist	Arl6IP1	Rescues ER disruption within axons and improves ER and mitochondrial organization within motor neurons, and improves locomotor ability [78].
Verapamil	sptz/CG5270	Reduced the number of autophagosomes accumulated, improved lysosomal function and autophagosome degradation, and rescued locomotor defects [73].
Bay K8644		
2′,5′-dideoxyadenosine		
SMER28		

biology that is important for understanding related rare and common diseases.

Our novel negative geotaxis monitoring output for slips, falls, and jumps is a tremendous advantage for modeling human disease related locomotion phenotypes. A recent study found patients with biallelic variants in *FICD* having common phenotypes of frequent falls, tiptoeing, walking difficulties, and progressive unsteady gait [6]. In our study, the coordinate matrix output for slips/falls/jumps is constrained within the duration of negative geotactic behavior. This precisely monitors only loss of coordination during intentional movement such as walking, rather than a general locomotion or balance phenotype, specifically pertaining to the disease phenotype as seen in patients. Interestingly, we observed a more severe phenotypes in falls/slips/jumps in males, suggesting a possible male vulnerability of loss of Fic, which may underly the fact that more male patients were reported.

FICD is the enzyme for post-translational AMPylation and deAMPylation modification [20]. So far the only substrate identified for FICD is BIP, an ER chaperone that regulates the UPRER [8–13]. The UPRER is essential for cell homeostasis, thus, any mutations to FICD or BIP will dramatically affect cellular physiology and pathology. There have been several studies performed to assess FICD and BIP functions. For example, *Drosophila* lacking FICD were viable and fertile, but blind due to compromised visual neurotransmission, assessed by electroretinogram [29,59]. In another study conducted, it was found that BIP null fly mutants die early in development and this lethality is rescued by including a copy of the genomic transgene expressing a wild-type or AMPylation-resistant mutant [29]. Overall, when BIP is AMPylated, the ER-transmembrane signaling molecules (ATF6, IRE1, and PERK) and ER-associated caspases (murine caspase-12/human caspase 4) are maintained in an inactive state through binding to GRP78 (BIP). After ER stress, such as protein misfolding, the survival pathways are activated to block further damage. However, when the stress is too severe, apoptotic responses are triggered, which eventually lead to cell death [15]. Our in vivo observation suggests that prolonged ER stress will lead to BIP upregulation as an early-stage response to ER stress. A previous in silico study has found that BIP clustering facilitates protein folding in the endoplasmic reticulum through cooperative action via entropic pulling where a greater degree of BIP clustering under conditions of ER stress was observed [60]. This is consistent with our findings of more small and intense BIP clusters in the *Fic* null mutants than that in controls as a result of increased ER stress in loss of Fic.

The current HSP treatments available are limited to physical therapy, oral antispastic drugs, botulinum toxin therapy, and surgical baclofen pump implantation. In this study, chemical chaperones PBA and TUDCA were tested as potential treatments to reduce the ER reactive oxygen species phenotype. PBA has been effective in children with urea-cycle disorders, and has been considered a promising candidate for the treatment of thalassemias, chemotherapy reagent, cystic fibrosis, and neurodegenerative diseases [56,57]. The mechanism of action is not fully understood, however, it is proposed in assisting protein folding by stabilizing the misfolded proteins, reducing their aggregation, assisting in transportation to the correct subcellular localization, as well as alleviating ER stress through HDAC inhibitor activity [56]. On the other hand, TUDCA has been effective in primary biliary cirrhosis and has an antiapoptotic mechanism by phosphorylation and inactivation of the proapoptotic factors, prevention of Bax translocation and cytochrome-C release, or stabilization of the lipid and protein structure of mitochondrial outer membranes [47,56]. In addition to blocking apoptosis, TUDCA appears to inhibit cell death by activating survival pathways such as p38/Erk/Mapk and PI3K signaling cascades [56]. In this study, we took advantage of the *Drosophila* nervous system and administered the chemical chaperones through diet, as well as treating patient-derived fibroblasts. We found that the chemical chaperones were able to improve the average speed at an early age, as well as the accumulation of reactive oxygen species both in vitro and in vivo, ameliorating the disease phenotype at an early stage. Due to the possibility of a long-term general toxicity, this indicates that the chemical chaperones may have an early therapeutic window, and further work is required to optimize the choice and dosage of chemical chaperones to achieve beneficial effects without long-term toxicity. Overall, our study underscores the utilization of a *Drosophila* model for HSP and the therapeutic potential of chemical chaperones including PBA for Hereditary Spastic Paraplegia.

4. Materials and methods

4.1. Drosophila stocks and experimental procedures

Flies were maintained on a cornmeal-molasses-yeast medium at 22 °C, 65 % humidity, with 12-h light/12-hour dark cycles. The following fly strains were used in the studies: w^{1118}, obtained from Bloomington *Drosophila* Stock Center (BDSC 3605), *UAS-mito-GFP/UAS-nls-GFP; R68A06-GAL4/Cd4tdTomato* (generated by recombining with BDSC 39449 [36]), and *w;* Fic^{30C}*;UAS-*Fic^{E247G} obtained from Dr. Helmut Kramer's laboratory [12,29].The Fic^{30C} mutant allele was generated by CRISPR on a w^{1118} background. The w^{1118} was hence used as the control for the experiment. The original stock obtained from the Kramer lab is the recombined Fic^{30C}*;UAS-*Fic^{E247G}. We have isolated the Fic^{30C} allele through backcrossing to w^{1118} strain. w^{1118} was used as a control for this study due to the background of Fic^{30C} stock line.

4.2. Antibodies and reagents

The following commercially available primary antibodies were used: rabbit anti-GRP78 (abcam, 108615, 1:250). The following secondary antibodies were used: Alexa Fluor Cy5-conjugated anti-rabbit secondary antibody (Rockland, 611-110-122, 1:300).

4.3. Fly dissection and immunohistochemical staining

Flies were dissected in phosphate-buffered saline (PBS, pH 7.4). Samples were fixed in 4 % formaldehyde for 15 min and washed in PBS containing 0.4 % v/v Triton X-100 (PBTX). Samples were then incubated with primary antibodies diluted in 0.4 % PBTX with 5 % normal goat serum at 4 °C overnight, followed by incubation with secondary antibodies diluted in 0.4 % PBTX with normal goat serum at 4 °C overnight, as well as DAPI staining (1:300, Invitrogen, D1306) at room temperature for 15 min. The samples were mounted on glass slides with VECTASHIELD Antifade Mounting Medium (Vector Laboratories).

4.4. Automated geotaxis monitoring

Behavior assay was performed using previously published methods [61]. Each vial was preloaded with ≤7 flies; the geotaxis of each fly was recorded with a digital camera (ImagingSource LLC, model no. DMK23U445). Matlab (Mathworks) was used for analysis. Individual fly vertical positions (maximum height, 14 cm) were used to calculate a cohort's climbing rate. Finally, the difference in SD of horizontal and vertical positions was used to calculate movement direction. Specifically, for a given fly, movement direction = (SD of y coordinates – SD of x coordinates)/(SD of y coordinates + SD of x coordinates). For slips/falls/jumps, the coordinate matrix output is taken from the fly tracking software and coordinates are removed after flies have reached the top of the vial because our interest pertains only to the negative geotactic behavior. The cutoff is within an average fly axis length (10 pixels) from the ROI defined at the top of the vial. Once the coordinates are pruned, the y-displacement of every frame is calculated by subtracting y-coordinates in a frame by the preceding frame. Slips, falls, and jumps are defined in terms of the average fly axis length in pixels. Slips are defined as 2–5 fly lengths (between −20 and −50 pixels), falls as 5+ fly lengths (<−50 pixels), and jumps as >2 fly lengths (+20 pixels). The number of instances of each action is summed for all tracks within the genotype of

interest and each sum is divided by the number of tracks to find the average instances per track.

4.5. Reactive oxygen species live imaging

ROS levels were assessed using live staining DHE, a fluorescent probe for superoxide and hydrogen peroxide.

4.5.1. DHE staining in Drosophila

Samples were dissected in warm Schneider's media, then incubated in 30 μM DHE for 15 min. The samples washed with PBS 3 times (5 min each), and a final wash with PBTX for 5 min. The samples were mounted on glass slides with VECTASHIELD Antifade Mounting Medium, and immediately imaged using an Olympus IX81 confocal microscope with oil immersion objective lens.

4.5.2. DHE staining in fibroblasts

Patient fibroblasts were obtained from previous study [6]. Fibroblasts were cultured in DMEM medium (Corning, 15-013-CV) supplemented with 10 % fetal bovine serum (ATCC, 30-2020) at 37 °C with 5 % CO_2 in the VWR symphony incubator. The cells were seeded in live cell image dishes (SPL Life Sciences, 200350) with 50 % confluence. 24 h later, the cells were treated with 2 mM PBA for 3 days. Then, the cells were washed with fresh medium and treated with 5 μM of DHE (Thermo, D11347) in 200 μL of fresh medium for 15 min and were imaged immediately. Images were processed using Olympus FluoView 10-ASW software and analyzed using ImageJ software.

4.6. Confocal image acquisition and processing

Slides were imaged using an Olympus IX81 confocal microscope with 20× or 40× oil immersion objective lens with a scan speed of 8.0 μs per pixel and spatial resolution of 1,024 × 1,024 pixels. Images were processed using FluoView 10-ASW (Olympus). Quantification was carried out using ImageJ/Fiji (1.53q;NIH).

4.7. Drug administration

Sodium phenylbutyrate (PBA) (Sigma, SML0309) or Tauroursodeoxycholic Acid (TUDCA) (EMD Millipore, 580549) was dissolved in water and then mixed into 10 mL of fly food at a final concentration of 2 mM and 10 mM, respectively. An equal amount of water was mixed into the fly food as a control. The vials were dried at room temperature for 12 h before feeding.

4.8. Statistics

No statistical methods were used to predetermine sample size. Data were analyzed Prism (Graphpad Software). Student's *t*-test was used for comparison of two groups. One-way ANOVA with Tukey's post-hoc corrections were used for comparison of more than two groups. $P < 0.05$ was considered statistically significant.

CRediT authorship contribution statement

Amanda G. Lobato: Writing – review & editing, Writing – original draft, Methodology, Investigation. **Natalie Ortiz-Vega:** Writing – review & editing, Methodology, Investigation. **Tijana Canic:** Writing – review & editing, Methodology, Investigation. **Xianzun Tao:** Writing – review & editing, Methodology, Investigation. **Nika Bucan:** Writing – review & editing, Investigation. **Kai Ruan:** Writing – review & editing, Investigation. **Adriana P. Rebelo:** Writing – review & editing, Investigation. **Rebecca Schule:** Writing – review & editing, Conceptualization. **Stephan Zuchner:** Writing – review & editing, Supervision. **Sheyum Syed:** Writing – review & editing, Methodology, Investigation, Funding acquisition. **R. Grace Zhai:** Writing – review & editing, Writing – original draft, Supervision, Project administration, Methodology, Investigation, Funding acquisition, Conceptualization.

Declaration of competing interest

Authors declare that they have no competing interests.

Data availability

Data will be made available on request.

Acknowledgements

We thank Zoraida Diaz-Perez for technical assistance. This work was supported in part by Solve-RD (the European Rare Disease Mechanisms and Models Consortium) grant Solve-RD-2020 (to RGZ), the National Institutes of Health/NCCIH grant R33AT010408 (to RGZ), and the National Science Foundation grant NSF#2131037 (to SS).

Appendix A. Supplementary data

Supplementary data to this article can be found online at https://doi.org/10.1016/j.bbadis.2024.167348.

References

[1] A. Mackay-Sim, Hereditary spastic paraplegia: from genes, cells and networks to novel pathways for drug discovery, Brain Sci. 11 (3) (2021).
[2] C. Blackstone, C.J. O'Kane, E. Reid, Hereditary spastic paraplegias: membrane traffic and the motor pathway, Nat. Rev. Neurosci. 12 (1) (2011) 31–42.
[3] K.R. Kumar, N.F. Blair, C.M. Sue, An update on the hereditary spastic paraplegias: new genes and new disease models, Mov Disord Clin Pract 2 (3) (2015) 213–223.
[4] C. Martinello, E. Panza, A. Orlacchio, Hereditary spastic paraplegias proteome: common pathways and pathogenetic mechanisms, Expert Rev. Proteomics 20 (7–9) (2023) 171–188.
[5] S. Gumeni, et al., Hereditary spastic paraplegia and future therapeutic directions: beneficial effects of small compounds acting on cellular stress, Front. Neurosci. 15 (2021) 660714.
[6] A.P. Rebelo, et al., BiP inactivation due to loss of the deAMPylation function of FICD causes a motor neuron disease, Genet. Med. 24 (12) (2022) 2487–2500.
[7] A. D'Amore, et al., Next generation molecular diagnosis of hereditary spastic paraplegias: an Italian cross-sectional study, Front. Neurol. 9 (2018) 981.
[8] S.A. Sieber, S. Cappello, P. Kielkowski, From young to old: AMPylation hits the brain, Cell Chem. Biol. 27 (7) (2020) 773–779.
[9] S. Preissler, et al., AMPylation matches BiP activity to client protein load in the endoplasmic reticulum, Elife 4 (2015) e12621.
[10] S. Preissler, et al., FICD acts bifunctionally to AMPylate and de-AMPylate the endoplasmic reticulum chaperone BiP, Nat. Struct. Mol. Biol. 24 (1) (2017) 23–29.
[11] A. Sanyal, et al., A novel link between Fic (filamentation induced by cAMP)-mediated adenylylation/ AMPylation and the unfolded protein response, J. Biol. Chem. 290 (13) (2015) 8482–8499.
[12] A.K. Casey, et al., Fic-mediated deAMPylation is not dependent on homodimerization and rescues toxic AMPylation in flies, J. Biol. Chem. 292 (51) (2017) 21193–21204.
[13] H. Ham, et al., Unfolded protein response-regulated Drosophila Fic (dFic) protein reversibly AMPylates BiP chaperone during endoplasmic reticulum homeostasis, J. Biol. Chem. 289 (52) (2014) 36059–36069.
[14] M. Kokkinidis, N.M. Glykos, V.E. Fadouloglou, Catalytic Activity Regulation Through Post-Translational Modification: The Expanding Universe of Protein Diversity, 2020, pp. 97–125.
[15] J. Wang, et al., HSPA5 gene encoding Hsp70 chaperone BiP in the endoplasmic reticulum, Gene 618 (2017) 14–23.
[16] M.S. Yasunori Kozutsumi, Karl Normington, Mary-Jane Gething, Joe Sambrook, The presence of malfolded proteins in the endoplasmic reticulum signals the induction of glucose-regulated proteins, Nature 332 (31) (1988) 462–464.
[17] W.-C. Weng, et al., Role of glucose-regulated protein 78 in embryonic development and neurological disorders, J. Formos. Med. Assoc. 110 (7) (2011) 428–437.
[18] L.A. Perera, et al., An oligomeric state-dependent switch in the ER enzyme FICD regulates AMPylation and deAMPylation of BiP, EMBO J. 38 (21) (2019) e102177.
[19] J. Fauser, et al., Specificity of AMPylation of the human chaperone BiP is mediated by TPR motifs of FICD, Nat. Commun. 12 (1) (2021) 2426.
[20] T.D. Bunney, et al., Crystal structure of the human, FIC-domain containing protein HYPE and implications for its functions, Structure 22 (12) (2014) 1831–1843.
[21] M.L.Y.K. Orth, AMPylation is a new post-translational modiFICation, Nat. Chem. Biol. 5 (6) (2009) 378–379.
[22] B.M. Adams, M.E. Oster, D.N. Hebert, Protein quality control in the endoplasmic reticulum, Protein J. 38 (3) (2019) 317–329.

[23] A.E. Frakes, A. Dillin, The UPR(ER): sensor and coordinator of organismal homeostasis, Mol. Cell 66 (6) (2017) 761–771.
[24] J.B. Summerville, et al., The effects of ER morphology on synaptic structure and function in Drosophila melanogaster, J. Cell Sci. 129 (8) (2016) 1635–1648.
[25] S. Xu, M. Stern, J.A. McNew, Beneficial effects of rapamycin in a Drosophila model for hereditary spastic paraplegia, J. Cell Sci. 130 (2) (2017) 453–465.
[26] Y. Lee, et al., Loss of spastic paraplegia gene atlastin induces age-dependent death of dopaminergic neurons in Drosophila, Neurobiol. Aging 29 (1) (2008) 84–94.
[27] N.C. O'Sullivan, et al., Reticulon-like-1, the Drosophila orthologue of the hereditary spastic paraplegia gene reticulon 2, is required for organization of endoplasmic reticulum and of distal motor axons, Hum. Mol. Genet. 21 (15) (2012) 3356–3365.
[28] C. Papadopoulos, et al., Spastin binds to lipid droplets and affects lipid metabolism, PLoS Genet. 11 (4) (2015) e1005149.
[29] A.T. Moehlman, et al., Adaptation to constant light requires Fic-mediated AMPylation of BiP to protect against reversible photoreceptor degeneration, Elife (2018) 7.
[30] H. Bolus, et al., Modeling neurodegenerative disorders in Drosophila melanogaster, Int. J. Mol. Sci. 21 (9) (2020).
[31] T. Gall, et al., Defining disease, diagnosis, and translational medicine within a homeostatic perturbation paradigm: the National Institutes of Health undiagnosed diseases program experience, Front Med (Lausanne) 4 (2017) 62.
[32] Y. Zhu, et al., Sorbitol reduction via govorestat ameliorates synaptic dysfunction and neurodegeneration in sorbitol dehydrogenase deficiency, JCI Insight 8 (10) (2023).
[33] R.J. Schilder, M. Raynor, Molecular plasticity and functional enhancements of leg muscles in response to hypergravity in the fruit fly Drosophila melanogaster, J. Exp. Biol. 220 (Pt 19) (2017) 3508–3518.
[34] M.A. Jones, M. Grotewiel, Drosophila as a model for age-related impairment in locomotor and other behaviors, Exp. Gerontol. 46 (5) (2011) 320–325.
[35] D. Rhodenizer, et al., Genetic and environmental factors impact age-related impairment of negative geotaxis in Drosophila by altering age-dependent climbing speed, Exp. Gerontol. 43 (8) (2008) 739–748.
[36] A. Jenett, et al., A GAL4-driver line resource for Drosophila neurobiology, Cell Rep. 2 (4) (2012) 991–1001.
[37] J.M. Blagburn, A new method of recording from the giant fiber of Drosophila melanogaster shows that the strength of its auditory inputs remains constant with age, PloS One 15 (1) (2020) e0224057.
[38] C.R. von Reyn, et al., A spike-timing mechanism for action selection, Nat. Neurosci. 17 (7) (2014) 962–970.
[39] Barret D. Pfeiffer, A.J., Ann S. Hammonds, Teri T.B. Ngo, Sima Misra, Christine Murphy, Audra Scully, Joseph W. Carlson, Kenneth H. Wan, Todd R. Laverty, Chris Mungall, Rob Svirskas, James T. Kadonaga, Chris Q. Doe, Michael B. Eisen, Susan E. Celniker, Gerald M. Rubin, Tools for neuroanatomy and neurogenetics in Drosophila, PNAS 105 (28) (2008) 9715–9720.
[40] N.L. Chanaday, E.T. Kavalali, Role of the endoplasmic reticulum in synaptic transmission, Curr. Opin. Neurobiol. 73 (2022) 102538.
[41] Z. Ozturk, C.J. O'Kane, J.J. Perez-Moreno, Axonal endoplasmic reticulum dynamics and its roles in neurodegeneration, Front. Neurosci. 14 (2020) 48.
[42] K. Yperman, M. Kuijpers, Neuronal endoplasmic reticulum architecture and roles in axonal physiology, Mol. Cell. Neurosci. 125 (2023) 103822.
[43] M.A. Tanouye, R.J. Wyman, Motor output of giant nerve fiber in Drosophila, J. Neurophysiol. 44 (1980) 405–421.
[44] D.G. King, R.J. Wyman, Anatomy of the giant fibre pathway in Drosophila. I. Three thoracic components of the pathway, J. Neurocytol. 9 (1980) 753–770.
[45] C.M. Ferencz, et al., Shaping the endoplasmic reticulum in vitro, Biochim. Biophys. Acta 1858 (9) (2016) 2035–2040.
[46] M.K. Brown, N. Naidoo, The endoplasmic reticulum stress response in aging and age-related diseases, Front. Physiol. 3 (2012) 263.
[47] A. Almanza, et al., Endoplasmic reticulum stress signalling - from basic mechanisms to clinical applications, FEBS J. 286 (2) (2019) 241–278.
[48] K.R. Bhattarai, et al., The aftermath of the interplay between the endoplasmic reticulum stress response and redox signaling, Exp. Mol. Med. 53 (2) (2021) 151–167.
[49] T. Konno, et al., Intracellular sources of ROS/H2O2 in health and neurodegeneration: spotlight on endoplasmic reticulum, Cells 10 (2) (2021).
[50] H.M. Zeeshan, et al., Endoplasmic reticulum stress and associated ROS, Int. J. Mol. Sci. 17 (3) (2016) 327.
[51] J. Wang, et al., Redox signaling via the molecular chaperone BiP protects cells against endoplasmic reticulum-derived oxidative stress, eLife (2014) 3.
[52] E. Owusu-Ansah, U. Banerjee, Reactive oxygen species prime Drosophila haematopoietic progenitors for differentiation, Nature 461 (7263) (2009) 537–541.
[53] K.K.G. Sergey Dikalov, David G. Harrison, Measurement of reactive oxygen species in cardiovascular studies, Hypertension 49 (4) (2007) 717–727.
[54] J.H. Jeon, et al., Chemical chaperones to inhibit endoplasmic reticulum stress: implications in diseases, Drug Des. Devel. Ther. 16 (2022) 4385–4397.
[55] S. Mimori, et al., Protective effects of 4-phenylbutyrate derivatives on the neuronal cell death and endoplasmic reticulum stress, Biol. Pharm. Bull. 35 (1) (2012) 84–90.
[56] F. Engin, G.S. Hotamisligil, Restoring endoplasmic reticulum function by chemical chaperones: an emerging therapeutic approach for metabolic diseases, Diabetes Obes. Metab. 12 (Suppl. 2) (2010) 108–115.
[57] X. Tao, et al., *Phenylbutyrate modulates polyamine acetylase and ameliorates Snyder-Robinson syndrome in a Drosophila model and patient cells.* JCI, Insight 7 (13) (2022).
[58] V. Debattisti, et al., Reduction of endoplasmic reticulum stress attenuates the defects caused by Drosophila mitofusin depletion, J. Cell Biol. 204 (3) (2014) 303–312.
[59] M. Rahman, et al., Visual neurotransmission in Drosophila requires expression of Fic in glial capitate projections, Nat. Neurosci. 15 (6) (2012) 871–875.
[60] M. Griesemer, et al., BiP clustering facilitates protein folding in the endoplasmic reticulum, PLoS Comput. Biol. 10 (7) (2014) e1003675.
[61] Y. Zhu, et al., *Sorbitol reduction via govorestat ameliorates synaptic dysfunction and neurodegeneration in sorbitol dehydrogenase deficiency.* JCI, Insight 8 (10) (2023).
[62] C. Blackstone, Cellular pathways of hereditary spastic paraplegia, Annu. Rev. Neurosci. 35 (2012) 25–47.
[63] S. Srivastav, et al., Atl (atlastin) regulates mTor signaling and autophagy in Drosophila muscle through alteration of the lysosomal network, Autophagy 20 (1) (2024) 131–150.
[64] S. Srivastav, et al., Motor neuron activity enhances the proteomic stress caused by autophagy defects in the target muscle, PloS One 19 (1) (2024) e0291477.
[65] C. De Gregorio, et al., Drosophila Atlastin in motor neurons is required for locomotion and presynaptic function, J. Cell Sci. 130 (20) (2017) 3507–3516.
[66] M. Lee, et al., Drosophila Atlastin regulates the stability of muscle microtubules and is required for synapse development, Dev. Biol. 330 (2) (2009) 250–262.
[67] N. Trotta, et al., The hereditary spastic paraplegia gene, spastin, regulates microtubule stability to modulate synaptic structure and function, Curr. Biol. 14 (13) (2004) 1135–1147.
[68] N.T. Sherwood, et al., Drosophila spastin regulates synaptic microtubule networks and is required for normal motor function, PLoS Biol. 2 (12) (2004) e429.
[69] G. Pareek, R.E. Thomas, L.J. Pallanck, Loss of the Drosophila m-AAA mitochondrial protease paraplegin results in mitochondrial dysfunction, shortened lifespan, and neuronal and muscular degeneration, Cell Death Dis. 9 (3) (2018) 304.
[70] P. Füger, et al., Spastic paraplegia mutation N256S in the neuronal microtubule motor KIF5A disrupts axonal transport in a Drosophila HSP model, PLoS Genet. 8 (11) (2012).
[71] I. Schmidt, et al., Kinesin heavy chain function in Drosophila glial cells controls neuronal activity, J. Neurosci. 32 (22) (2012) 7466–7476.
[72] J.J. Perez-Moreno, et al., Drosophila SPG12 ortholog, reticulon-like 1, governs presynaptic ER organization and Ca2+ dynamics, J. Cell Biol. 222 (6) (2023).
[73] C. Vantaggiato, et al., Rescue of lysosomal function as therapeutic strategy for SPG15 hereditary spastic paraplegia, Brain 146 (3) (2023) 1103–1120.
[74] Y. Tian, et al., Tissue-autonomous function of Drosophila seipin in preventing ectopic lipid droplet formation, PLoS Genet. 7 (4) (2011) e1001364.
[75] M. Nahm, et al., Spartin regulates synaptic growth and neuronal survival by inhibiting BMP-mediated microtubule stabilization, Neuron 77 (4) (2013) 680–695.
[76] B. Napoli, et al., Naringenin ameliorates Drosophila ReepA hereditary spastic paraplegia-linked phenotypes, Front. Neurosci. 13 (2019) 1202.
[77] F. Mandik, et al., A new model for fatty acid hydroxylase-associated neurodegeneration reveals mitochondrial and autophagy abnormalities, Front. Cell Dev. Biol. 10 (2022) 1000553.
[78] D.J. Byrne, et al., Liver X receptor-agonist treatment rescues degeneration in a Drosophila model of hereditary spastic paraplegia, Acta Neuropathol. Commun. 10 (1) (2022) 40.
[79] P.C. Fowler, et al., Loss of the mitochondrial fission GTPase Drp1 contributes to neurodegeneration in a Drosophila model of hereditary spastic paraplegia, Brain Sci. 10 (9) (2020).
[80] E. Panza, A. Meyyazhagan, A. Orlacchio, Hereditary spastic paraplegia: genetic heterogeneity and common pathways, Exp. Neurol. 357 (2022) 114203.
[81] G. Orso, et al., Disease-related phenotypes in a Drosophila model of hereditary spastic paraplegia are ameliorated by treatment with vinblastine, J. Clin. Invest. 115 (11) (2005) 3026–3034.
[82] C. Julien, et al., Conserved pharmacological rescue of hereditary spastic paraplegia-related phenotypes across model organisms, Hum. Mol. Genet. 25 (6) (2016) 1088–1099.